Ultrasonics 97 (2019) 1–10

Contents lists available at ScienceDirect

Ultrasonics

journal homepage: www.elsevier.com/locate/ultras

Nonlinear ultrasonic test of concrete cubes with induced crack

Mingjie Zhao[a,b,*], Zhichao Nie[a], Kui Wang[a,b], Pan Liu[a], Xin Zhang[a]

[a] Key Laboratory of Hydraulic and Waterway Engineering of Ministry of Education, Chongqing Jiaotong University, Chongqing 400074, China
[b] Engineering Research Center of Diagnosis Technology and Instruments of Hydro-Construction, Chongqing Jiaotong University, Chongqing 400074, China

ARTICLE INFO

Keywords:
Second and third harmonic ratios
Concrete
Crack
Excitation voltage
Crack orientation

ABSTRACT

Second and third harmonic ratios method to evaluate initial damage in concrete have been extensively studied. However, some regularities of this technique still not clear in current stage. In order to better understand the regularity of nonlinear parameters β and γ on micro and macro damage in concrete, the cracks with different damage scales are induced in concrete specimens. Three levels of test voltage are applied to intact concrete specimens, with the purpose to demonstrate the excitation voltage has an unneglectable effect on nonlinear parameters. The regularity of nonlinear parameters on crack orientation is also obtained in this study. The results of the experiment have considerable importance with respect to the method of higher harmonic ratios for concrete and other inhomogeneous materials.

1. Introduction

Present studies reveal that early damage, e.g., micro cracks, appear commonly in concrete, even in well-made concrete samples [1]. Micro cracks are crucial in the failure process. The traditional ultrasonic tests for the generation and development of micro cracks have limitations. For example, the method utilising wave velocities is incapable of micro structure evaluation of concrete. X-ray diffraction (XRD) and scanning electron microscopy (SEM) are expensive and inconvenient in civil engineering [2,3]. Therefore, it is necessary to develop more precise and efficient method to characterize the appearance and development of micro cracks in concrete. The new methods can complement and improve the traditional ultrasonic techniques [4–6].

Classical nonlinear acoustics theory shows that second harmonics are mainly induced by an harmonicity of the crystal lattice of materials [7–9]. The nonlinear ultrasound research can be simply classified as follow: methodology of the test and evaluation [5,10,11], sensitivity verification of the method for micro damage [12–14], prediction of residual life of materials [15,16], and nonlinear ultrasound imaging [17]. Nonclassical nonlinearity effect is caused by micro defects (cracks, pores) in geomaterials [18], and it is usually considered stronger than the classical nonlinearity. Nonclassical nonlinear models mainly include contact surface model, hysteresis model, and bilinear stiffness model [19]. Based on them, Zhao et al. deduced an analytical expression of nonlinear parameter and elastic moduli of solid [20] and verified the theoretical model with numerical simulations. Nam et al. proposed a theoretical model to evaluate with the amplitude of the second harmonic the micro damage located at both inner and outer surfaces of the structure [21].

In order to explore nonlinear ultrasonic response of the concrete under different load patterns, Ongpeng et al. carried out nonlinear ultrasonic tests under loading-unloading situations on concrete specimens with different water cement ratios. The results show that third-order harmonics are more sensitive to the uniaxial compression pattern, while second-order harmonics are more sensitive under the multiple load and unload pattern [22]. With Scaling Subtraction method, Antonaci et al. effectively evaluated the mechanical evolution related to the imperfect bonding interface in concrete under uniaxial compression [23]. Overall, the nonlinear ultrasonic techniques have become one of the most powerful methods in the initial damage detection of bonding materials and geomaterials [12,24,25].

The objective of this research is to explore the regularity of the second and third harmonic ratios on multiscale damage. For this purpose, concrete specimens containing multiscale cracks distributed along the height are made in the experiment, and the nonlinear parameters β and γ are used to evaluate the damage degree. The results show that the higher harmonic ratios method is sensitive to the presence of micro crack. The wave velocity method is also used to confirm the degree of damage in cracked concrete specimens. In addition, the influence of oblique angle between incident wave and micro crack is studied in this experiment.

* Corresponding author at: Key Laboratory of Hydraulic and Waterway Engineering of Ministry of Education, Chongqing Jiaotong University, Chongqing 400074, China.
E-mail address: m.j.zhao@163.com (M. Zhao).

https://doi.org/10.1016/j.ultras.2019.04.002
Received 6 November 2018; Received in revised form 2 April 2019; Accepted 2 April 2019
Available online 03 April 2019
0041-624X/

2. Generation of high-order harmonics

According to the linear acoustic theory, when a one-dimensional longitudinal wave propagates in an isotropic media, the amplitude of the elastic wave is small, and the stress-strain relation is linear. Therefore, the test parameters, i.e., the wave velocity v and amplitude of the head wave A are insensitive to the changes of the micro structure and to the presence of microcracks in the material. In nonlinear elastic theory, the stress-strain relation does not satisfy the linear assumption anymore.

While with the nonlinear wave equation, for one dimensional case, the solution of the nonlinear wave equation can be written as [26].

$$u = u_0 + u' = A_1 \cos(kx - \omega t) + \frac{A_1^2 k^2 x \beta}{8} \cos(2kx - 2\omega t) + \ldots \quad (1)$$

where, u_0 is the linear solution, u' is the nonlinear solution, A_1 is the amplitude of fundamental waves, A_2 is the amplitude of second harmonics, $k = \omega/c$ is the wave number, and β is the second-order nonlinear parameter. The relationship of the amplitude of fundamental wave and harmonic can be expressed as

$$\beta = \frac{8A_2}{A_1^2 k^2 x} \quad (2)$$

In experiments, the parameter β is usually used to replace β because the measurement of the absolute motion displacement at the receiver is inconvenient. The expression of β is

$$\beta = \frac{A_2}{A_1^2} \quad (3)$$

It should be point out that the value of β depends not only on the damage degree of the materials, but also on the propagating distance and the wave number. The wave number is controlled by the excitation source, and the propagation distance must be constant or quantitatively changed according to the aim of study.

Similarly, by extending the stress-strain equation to the third order, the third-order nonlinear parameter can be defined as follows

$$\gamma = \frac{32A_3}{A_1^3 k^4 x^2} \quad (4)$$

$$\gamma' = \frac{A_3}{A_1^3} \quad (5)$$

Throughout the paper, the notation of β and γ will be used to replace β' and γ', i.e., $\beta = \frac{A_2}{A_1^2}$* MERGEFORMAT and $\gamma = \frac{A_3}{A_1^3}$* MERGEFORMAT.

3. Experimental procedure

3.1. Concrete specimens

In this experiment, two groups of cubic concrete specimens have been prepared. One group is intact (C1 ~ C5) and the other is cracked (D1 ~ D3) (Fig. 1). The size of the concrete specimens is 200 mm × 200 mm × 200 mm. The mixture proportions of concrete specimens are given in Table 1. The procedure for damage generation is the following [27]. Firstly, after pouring of concrete, a thin steel sheet with machine oil on the surface is vertically penetrated into the concrete mixture. The length, width and thick of the steel sheet is 100 mm, 80 mm, and 2 mm. The insertion depth is 100 mm at different angles in order to generate 30°, 45° and 90° preexisting cracks, respectively. One hour later, the steel sheet is removed out of the specimen carefully. Then an artificial crack is left in the specimen, with damage distributed along the height direction. After the cracked concrete curing, a wire with a diameter equal to 0.8 mm is plugged into each crack, and the homogeneity of the crack along its longitudinal direction is examined by repeating this operation at different positions. The wire remains vertical during the whole process. The maximum measured extension length is 45 mm. The general open degree of the semi-penetrating crack can be obtained as Fig. 2.

Table 1
Details of mixture proportions of the concrete specimens[a].

Design Compressive strength (MPa)	Maximum size of gravel (mm)	W/C (%)	Unit quantity (kg/m^3)				Average P-wave velocity/(m/s)[b]
			Water	Cement	Sand	Gravel	
30	30	46	190	480	640	1034	4114

[a] The concrete mix and compressive strength are designed in accordance with the JGJ 55-2011 [28].
[b] The wave velocity test was carried out on five intact specimens.

A number of test points are arranged on the surface of the specimens, being-their locations strictly limited because the transmitter and receiver should be aligned. Minor defects existing on the surface of the concrete, which might lead to coupling errors. To avoid them, the surface should be as flat as possible. Therefore, mortar and sandpaper have been used to polish the surface of the concrete.

3.2. Experimental system

GSC-1 ultrasonic instrument is used in this experiment. The ultrasonic instrument is highly integrated and works with an external computer for the pulse transmitting and receiving. The experimental set-up is shown in Fig. 3. High-frequency ultrasonic has a better resolution to the damage of materials, but the attenuation is too strong when high-frequency waves propagate in concrete. The penetration of the ultrasonic waves is small. In this study, the generation frequency of the pulse signals is chosen as 47 kHz, and the sampling rate recording the receiving signals is set to 5 MSa/s. Three levels of output peak voltage namely, 500, 750, and 1000 V, are chosen in the experiments. A compressional ultrasonic transducer with 50 kHz center frequency is used for excitation. A receiver with 70 kHz center frequency is used at the receiving end. The performances of the transducers are listed in

(a) Intact (b) 30 ° crack (c) 45 ° crack (a) 90 ° crack

Fig. 1. Intact and cracked concrete specimens.

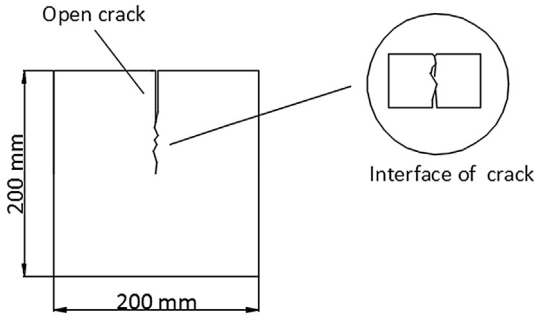

Fig. 2. Schematic representation of the morphology of the crack.

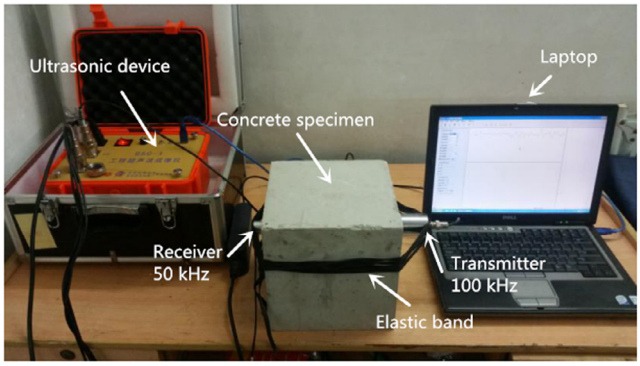

Fig. 3. Test system for signal generation and acquisition.

Table 2
The basic parameters of the transducers used in this experiment.

Purpose	Model	Center frequency (kHz)	Bandwidth (kHz)	Diameter (mm)
Transmitting	KCRT816	50	45–55	38
Receiving	PXR07	70	40–180	22

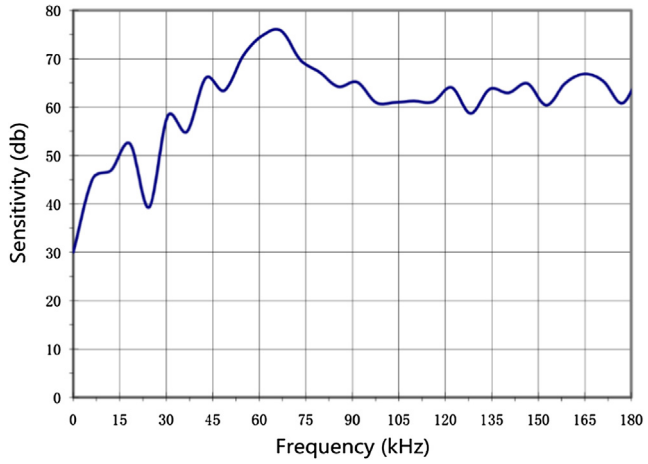

Fig. 4. Schematic diagram of frequency response of pxr07 transducer.

Table 2. The broadband transducer used in this experiment has a good response to the second and third harmonics considering that the sensitivity at $2f_0$ and $3f_0$ reaches 60 db (Fig. 4). Fig. 5 shows the received time domain signal for one of the intact specimens and the Fourier spectra. Second and third harmonics are exhibited in the Fourier spectra.

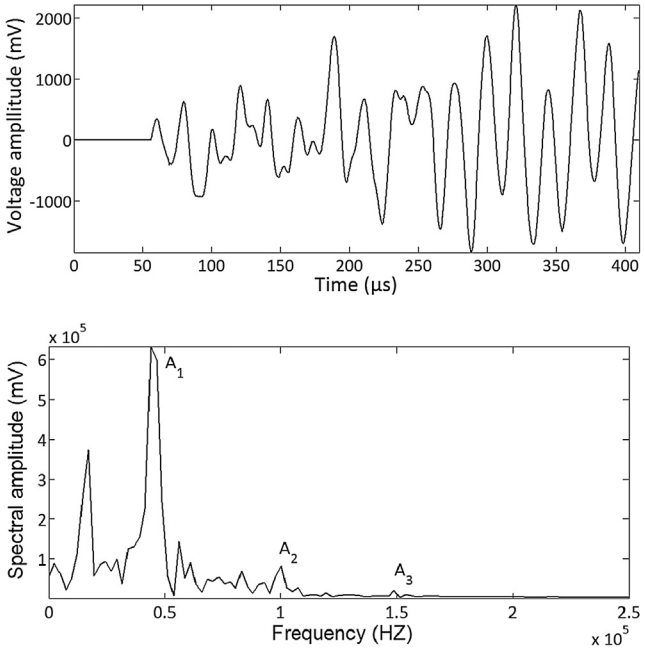

Fig. 5. Test signal recorded and frequency spectra of the received signal.

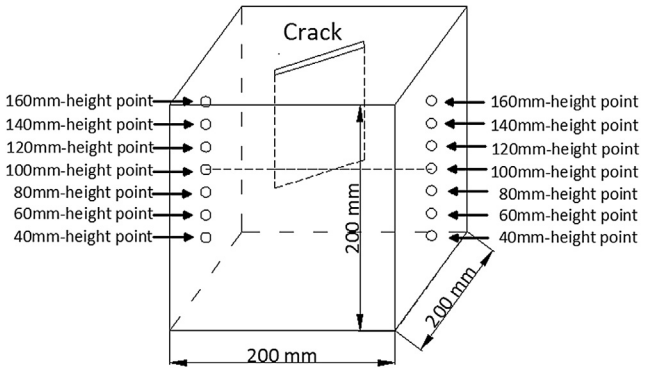

Fig. 6. The test point arrangement in the case of the cracked concrete.

3.3. Arrangement of the test points

As shown in Fig. 6, seven test points are arranged for each cracked specimen. The test points with an interval of 20 mm are distributed from 40 to 160 mm-height from the bottom of the specimen. The acute angle between the direction of propagation of the ultrasonic wave and the preexisting crack is defined as the crack angle in this article. Tests for specimens with 0° and 60° cracks are carried out locating transducers on the proper opposite surfaces of the specimens with 90° and 30° cracks. Globally, the tests for concrete specimens with 0°, 30°, 45°, 60°, and 90° cracks are carried out in this experiment. Thus, there are 7 test points for each cracked specimen, and a total of 35 sets of test signals are obtained. For each intact specimen, 60 and 140 mm-height positions are tested under three levels of voltage, and a total of 30 sets of test signals are obtained.

More details about the transducer coupling are introduced as follows. Firstly, the diameters of the transmitter and the receiver are measured. And the transducers are fixed on the specific position. In addition, prior to applying the couplant to the transducers and the surface of the specimen, the dust adhering to the surface is wiped to keep the contact surface completely clean. By applying adequate Vaseline, the transducer is tightly attached on the surface of the concrete. Then the extra couplant left on the edge of the transducers is wiped off. And the specimen and transducers are winded with an elastic

Table 3
The second-order nonlinear parameter measured at different test points on intact specimens. (The superscript on β represent the serial number of the specimen, and the subscript represent the test point).

Peak voltage/V	$\beta_2^1/*10^{-6}$	$\beta_6^1/*10^{-6}$	$\beta_2^2/*10^{-6}$	$\beta_6^2/*10^{-6}$	$\beta_2^3/*10^{-6}$	$\beta_6^3/*10^{-6}$	$\beta_2^4/*10^{-6}$	$\beta_6^4/*10^{-6}$	$\beta_2^5/*10^{-6}$	$\beta_6^5/*10^{-6}$	Mean $\bar{\beta}$ $/*10^{-6}$	Standard deviation $\sigma_1/*10^{-6}$
500	0.60	0.64	1.47	0.97	0.37	0.96	0.24	0.56	0.71	0.82	0.74	0.33
750	0.44	0.44	0.78	0.63	0.25	0.77	0.19	0.40	0.46	0.54	0.49	0.18
1000	0.25	0.53	0.51	0.35	0.25	0.43	0.15	0.44	0.35	0.29	0.36	0.11

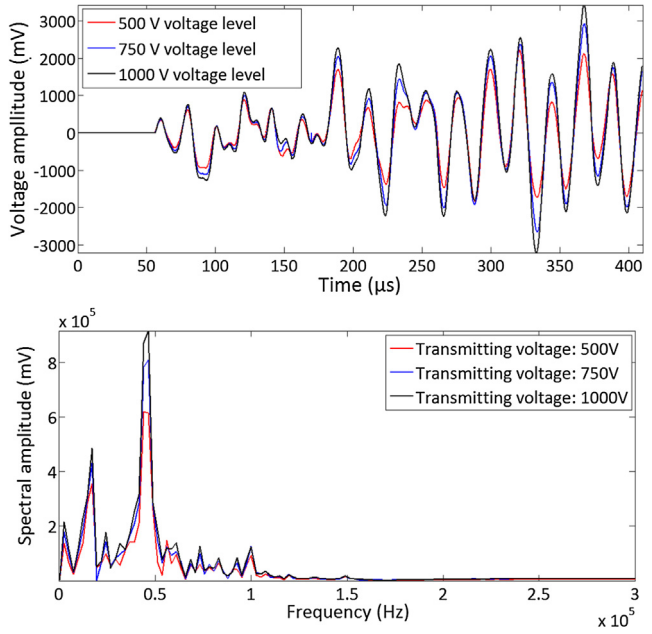

Fig. 7. Time domain signal and frequency spectra of received signals with 500, 750 and 1000 V excitation voltage.

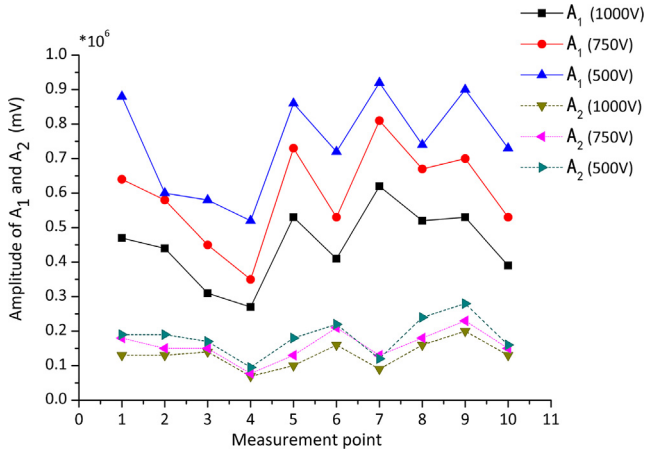

Fig. 8. The distribution of fundamental and second harmonic amplitude of the five intact specimens.

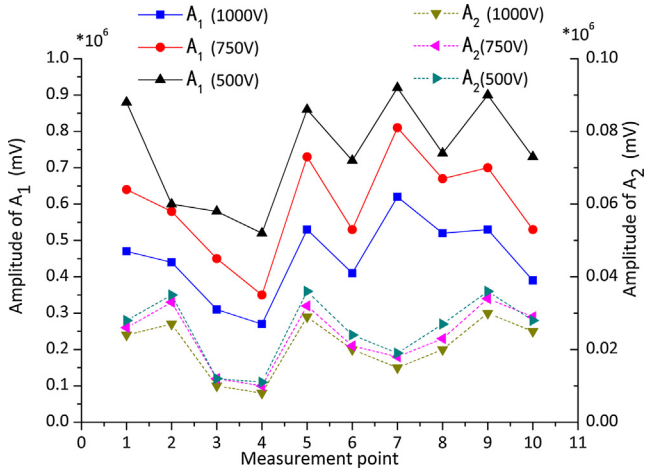

Fig. 9. The distribution of fundamental and third harmonic amplitude of the five intact specimens.

band. To avoid that the original position might be changed because of other operations before the signal excitation (e.g., wiping off couplant around the transducer, winding elastic band), the fixation position of the transducers was checked once more before the excitation and reception of the signals.

4. Experimental results

4.1. Nonlinearity parameters β and γ in intact concrete

Five intact concrete specimens are tested according to the configuration described above. The results are listed in Table 3 and reveal that the value of β is closely correlated to the supplied voltage. The higher voltage level, the smaller corresponding β is calculated. On the other hand, β always fluctuates at a certain level, indicating that even for an intact concrete specimen, the values of β are different at different test points. The primary reason is that the composition of the concrete has strong randomness and discreteness. It is also found that although the minor defects on the surface of the concrete are repaired with mortar and sandpaper before the test, the coupling problem still exists in this experiment, resulting some accidental errors on β. Therefore, in further studies, an air transducer should be used to reduce coupling errors [14,29].

Moreover, the 1000 V voltage achieves the smallest standard deviation of β compared with the results at 500 and 750 V voltages. This

Table 4
The third-order nonlinear parameter measured at different test points on intact specimens. (The superscript on γ represent the serial number of the specimen, and the subscript represent the test point).

Peak voltage/V	$\gamma_2^1/*10^{-13}$	$\gamma_6^1/*10^{-13}$	$\gamma_2^2/*10^{-13}$	$\gamma_6^2/*10^{-13}$	$\gamma_2^3/*10^{-13}$	$\gamma_6^3/*10^{-13}$	$\gamma_2^4/*10^{-13}$	$\gamma_6^4/*10^{-13}$	$\gamma_2^5/*10^{-13}$	$\gamma_6^5/*10^{-13}$	Mean $\bar{\gamma}$ $/*10^{-13}$	Standard deviation $\sigma_2/*10^{-13}$
500	2.31	3.18	3.48	4.28	1.93	2.92	0.65	1.36	2.08	4.17	2.64	1.12
750	1.00	1.64	1.36	2.31	0.84	1.46	0.35	0.75	0.98	1.93	1.26	0.56
1000	0.42	1.62	0.64	0.80	0.57	0.66	0.25	0.66	0.49	0.72	0.68	0.35

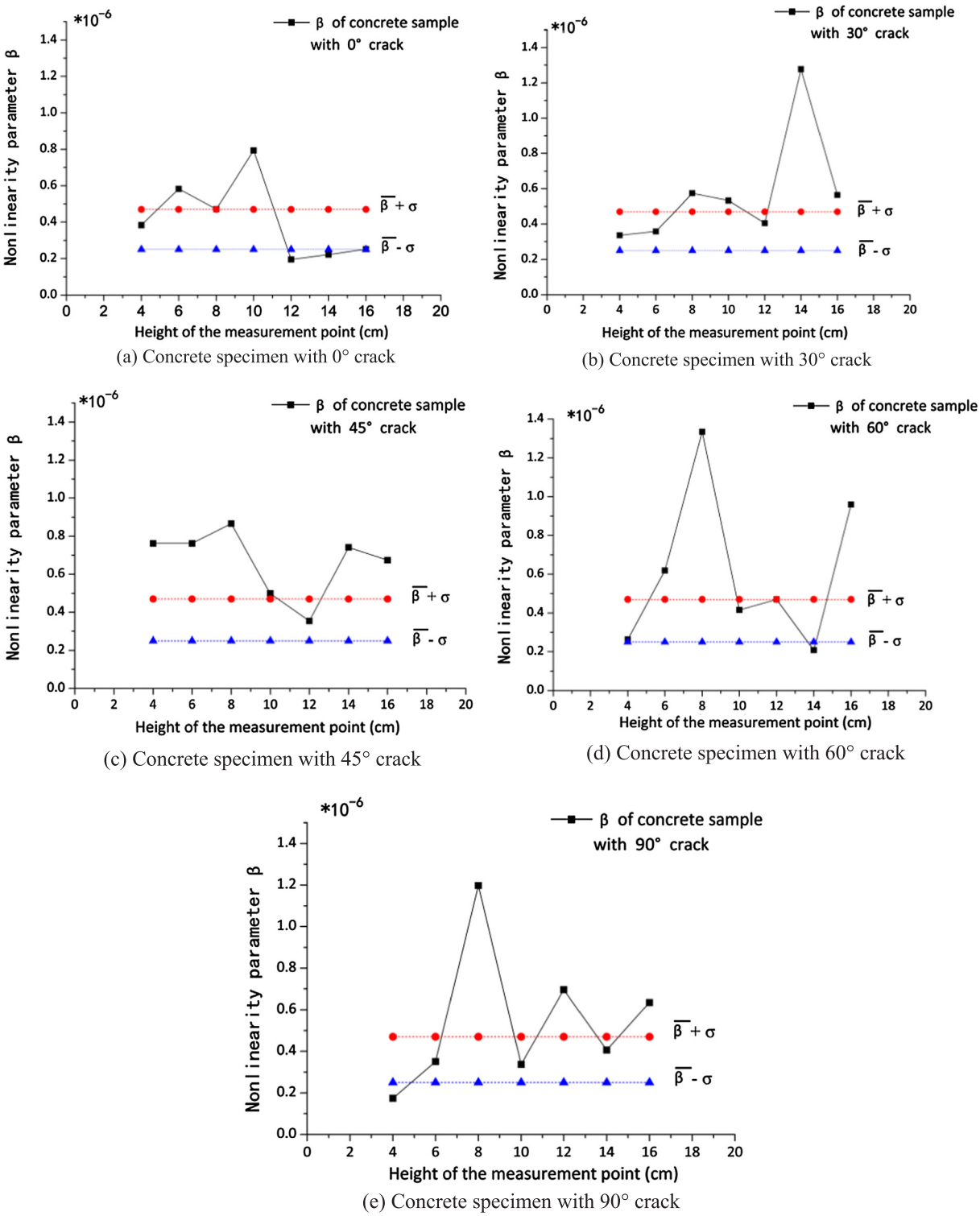

Fig. 10. The distribution of non-linearity parameter β on concrete specimens with 0°, 30°, 45°, 60° and 90° cracks.

indicates that the values of β in this group are more centralized, meaning results are more stable. Thus, it can be concluded that the 1000 V voltage is most suitable for this experiment. In order to prove the excitation amplitude definitely have greater influence on β than other errors, the received time domain and the frequency spectra at three levels of excitation voltage are shown in Fig. 7. The higher voltage can be regarded as an amplification of the fundamental and higher order harmonics at the lower voltage. However, this amplification is not constant in the whole frequency domain. The increase of A_1 is lager than of A_2, which can also be noticed in Fig. 8. The conclusion is not contradictory to the existing research [30,31], since the amplitude of second harmonics positively gets larger at higher voltage levels.

The third-order nonlinear parameter γ are also analyzed in same way, and similar conclusions can be drawn. The value of γ decreases with the increase of the excitation voltage. And strong fluctuations can also be observed in Table 4 and Fig. 9. The same conclusion that 1000 V is more appropriate in this experiment can be drawn.

When comparing with the second harmonic ratio β, the third

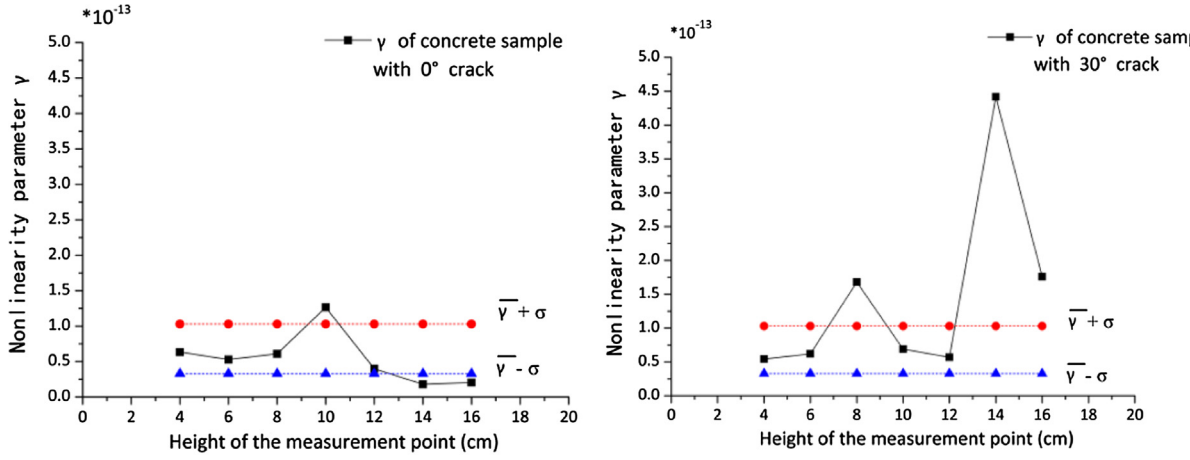

(a) Concrete specimen with 0° crack

(b) Concrete specimen with 30° crack

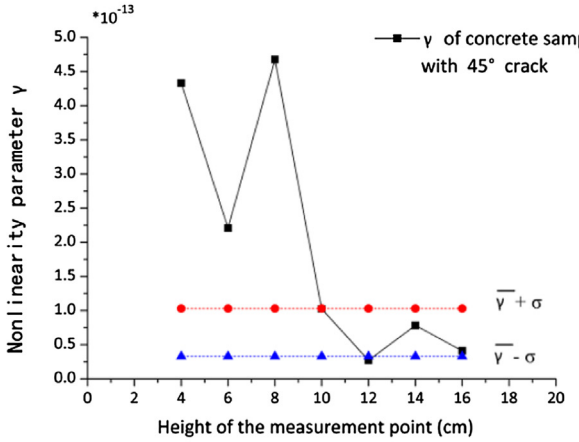

(c) Concrete specimen with 45° crack

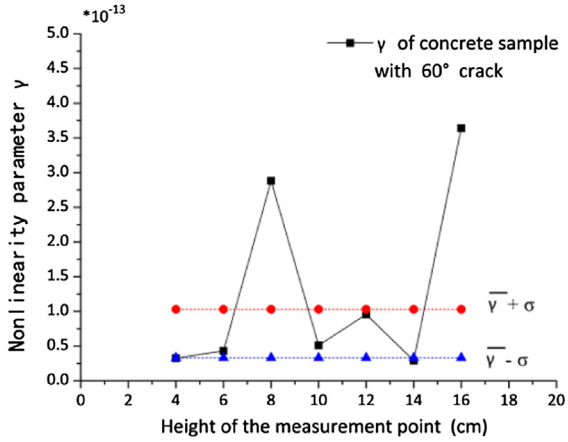

(d) Concrete specimen with 60° crack

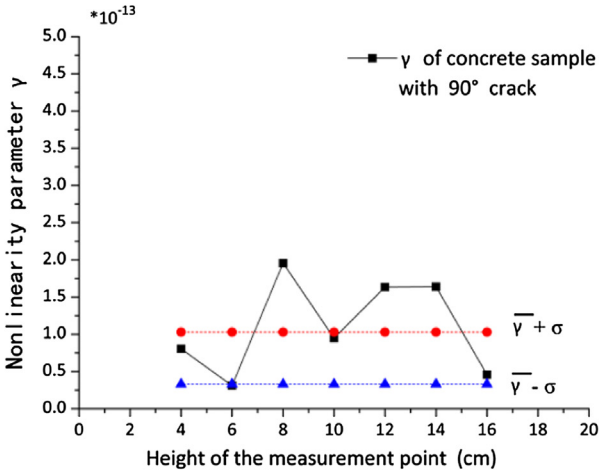

(e) Concrete specimen with 90° crack

Fig. 11. The distribution of non-linearity parameter γ on concrete specimens with 0°, 30°, 45°, 60° and 90° cracks.

harmonic ratio γ varies at a higher rate as evinced from its larger standard deviation. In recent years, studies on the comparison between the second and third harmonic ratios have concluded that both non-linear parameters follow a similar behaviour for the same damage evolution in concrete, but the third harmonic ratio is more sensitive [22,32,33]. To improve the reliability of the experimental results, the second and third harmonic ratios are both used to evaluate damage in concrete specimens.

4.2. Nonlinearity parameters β and γ in cracked concrete

The results of our experiments are plotted in Figs. 10 and 11. Due to micro defects randomly distribute in concrete specimens, the β and γ obtained at different test points on the cracked specimens is diverse.

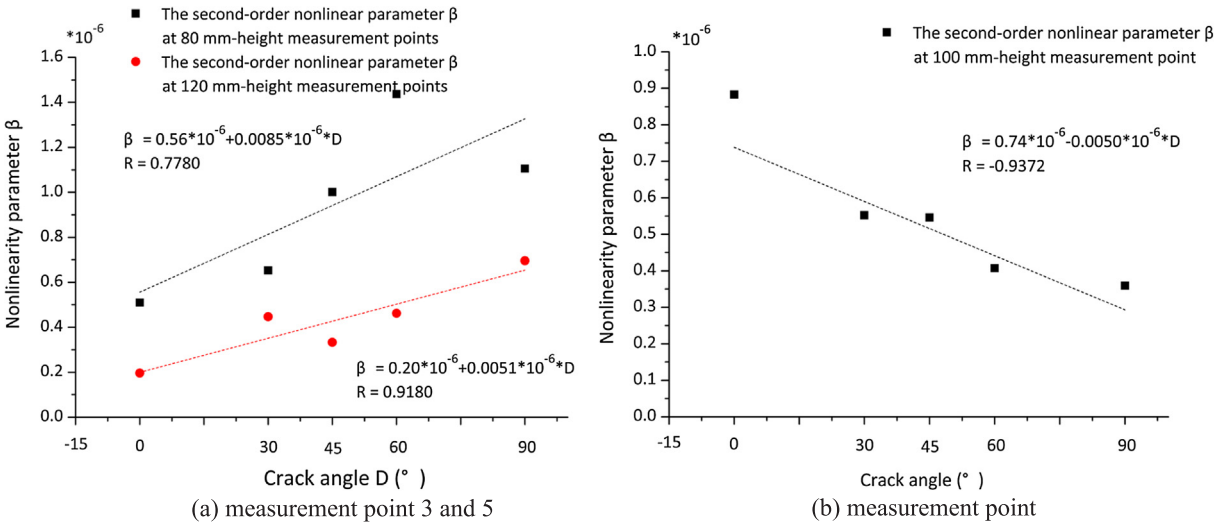

Fig. 12. The β varies with crack angle (R is Pearson correlation coefficient).

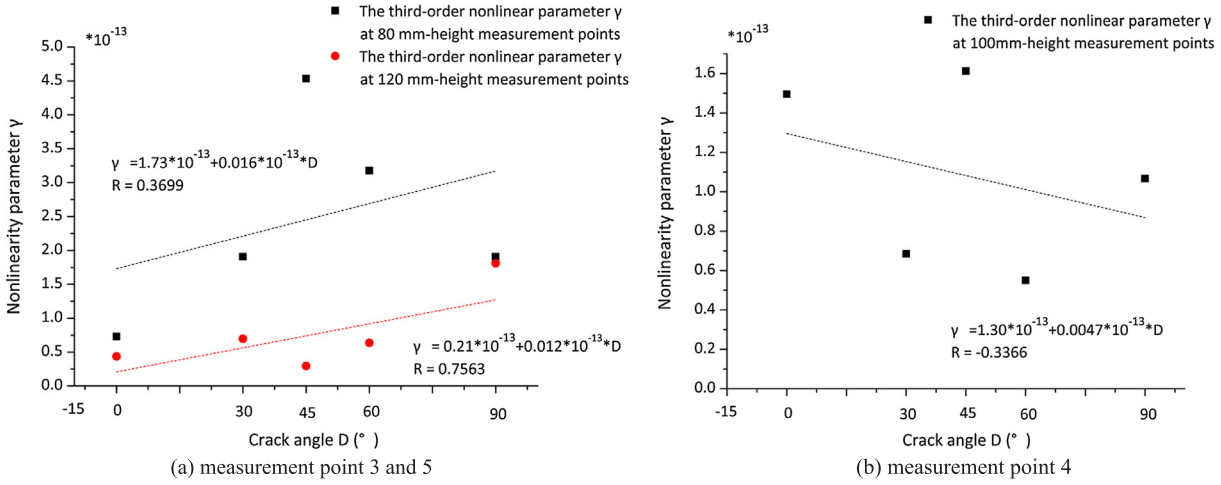

Fig. 13. The γ varies with crack angle (R is Pearson correlation coefficient).

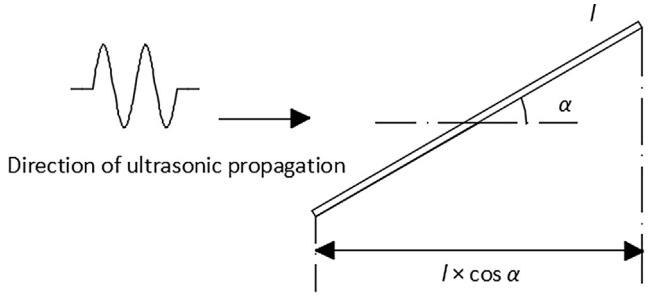

Fig. 14. Diagram of ultrasonic waves passing through the oblique crack.

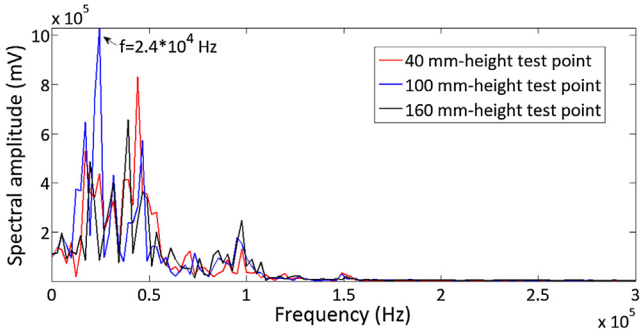

Fig. 15. Fourier spectra at 40, 100 and 160 mm-height measurement points.

Nevertheless, several results about the regularity of damage degree and angles on nonlinear parameters β and γ can still be extracted. To appreciate which test points behave differently from linear ones, the band which boundaries defined by $\bar{\beta} \pm \sigma_1$ and $\bar{\gamma} \pm \sigma_2$ are plotted in each subplot. The $\bar{\beta}$, $\bar{\gamma}$, σ_1 and σ_2 represent the means and standard deviations of nonlinear parameters β and γ in intact concrete specimens. It can be observed that each band is located at the lower position of the subplot, indicting nonlinear parameters β and γ are effective to characterize the appearance of micro damage in concrete. Besides, the concrete specimens are considered intact at 40 mm- and 60 mm-height, since the first two points are mostly into or nearby the band. Among the seven test points for each cracked specimen, 80 mm-height test point shows a clear upward trend compare with 40 and 60 mm-height test points. The main reason is that after removing the steel sheet above 100 mm-height of the specimen, the segregation occurs around 80 mm-height, and the uniformity and continuity of this point are affected. Because the microscopic damage is locally generated, a stronger nonlinear ultrasonic effect appears when ultrasonic waves pass through this area. On the other hand, above 100 mm-height, the distance between the crack surfaces is likely larger than the maximum displacement of the waves. Thus, ultrasonic waves cannot directly pass through the crack, and no

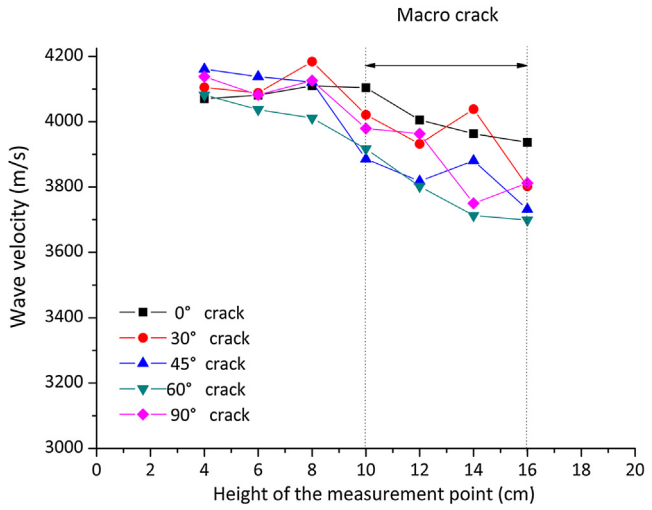

Fig. 16. Schematic diagram of wave velocity variation at different test point of cracked concrete.

Table 5
Wave velocity at each test point on cracked specimens.

Crack angle (°)	0	30	45	60	90
Average wave velocity of test points 1–3 (m/s)	4087	4126	4140	4043	4115
Average wave velocity of test points 5–7 (m/s)	3968	3924	3807	3738	3841

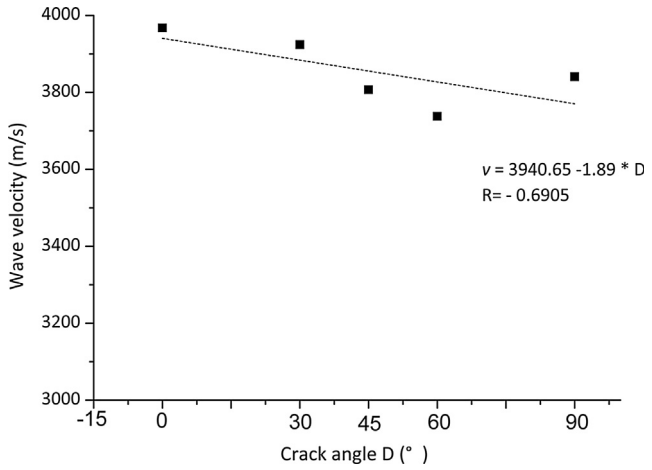

Fig. 17. Average wave velocity of 120, 140 and 160 mm-height test points on the specimens with 0°, 30°, 45°, 60° and 90° crack.

contact acoustic non-linearity is generated. Only a small amplitude of second (third) harmonic can be generated at the micro cracks internal to concrete. Besides, the A_1 is significantly affected by the attenuation and scattering feature of the linear waves at notch. As a result, the β and γ decrease in general when the damage is at macro scale [34]. It is still very difficult to use β and γ for characterizing macro damage in concrete. More experimental and theoretical should be carried out to find out the regularity of β and γ in relation to the macro cracks.

As mentioned above, the segregation occurred when crack induced in concrete. The segregation of concrete is an important phenomenon during construction for assuring design strength and durability, and it is affected by a lot of factors, such as specific surface area of aggregates, mortar viscosity, et al [35–37]. Since nonlinear parameters β and γ are sensitive to micro cracks and pores in concrete, they also have great potential in evaluating manufacture quality of concrete. More studies should be carried out on characterizing the degree of segregation in concrete with higher harmonic ratios method.

4.3. Non-linearity parameters β and γ in concrete with different angles

In this experiment, the relationships between the crack angles and β (γ) are studied by analyzing five types of cracked specimens at 80, 100 and 120 mm-height points. The results are shown in Figs. 12 and 13. According to the Pearson correlation coefficient R and the slop of each linear regression line, it can be concluded that the parameters β and γ depends only roughly in a linear way from crack angle D. A Linear fitting (straight lines) is nevertheless satisfactory and the slope characterises the general trend. As discussed above, the β and γ at 80 mm-height point are larger than those at 120 mm-height and increase with the crack angle. The relevant reasons have been explained in previous section. However, the 100 mm-height point exhibits an opposite tendency comparing with the 80 and 120 mm-height points. Remarkably, Yang et al. has obtained a similar conclusion with numerical simulation. When the crack is parallel to the propagation direction of the waves, the amplitude of second harmonic is so small that the micro crack cannot be detected [38]. The experimental results indicate that although at 80 and 120 mm-height we observe similar regularity, the damage degree at two points is quite different. At the 80 mm-height, the microscopic damage is caused by the healing of the upper mixture, which should be regarded as an inhomogeneity and contact-type defects of material. On the contrary, a macroscopic crack with a strong discontinuity exists at 120 mm-height. A different explanation is needed for results at 100 mm-height. As the crack angle decreases, the value of β and γ gradually reduce because of the shorter overlapping length of the wave propagation path and the bottom boundary of the crack, resulting in the so-called “boundary effect”. As shown in Fig. 14, where α is the crack angle, when the crack angle is 0, the overlapping distance between the wave propagation path and the bottom boundary of the crack is longest. It means the most disturbance produce to the acoustic waves in such a case. As the crack angle increase, the length of the bottom boundary along the direction of ultrasonic propagation will decrease, and little disturbance occur when the crack angle is 90°. Thus, the related nonlinear parameters β and γ are the smallest.

To better support our explanation, another phenomenon observed in experiments is discussed in this section. For all cracked specimens, the dominant frequency shifts to a low-frequency zone in Fourier spectra at 100 mm-height point, namely, $f_0 = 24$ kHz (Fig. 15). This effect is not found in intact specimens. In addition, as the transmitter and the receiver move upward, the dominant frequency gets back to the normal. There are two accounts might be reasonable for this phenomenon: divergence of frequency [39–41] and “CAN” effect [42,43]. As for the divergence of frequency, it is indicated that the frequency spreading from a wider spectrum once concrete at low levels of load, and high frequencies become ever more attenuated with accumulation of damage. The CAN model is used to explain the generation of subharmonics and higher harmonics. When ultrasonic waves pass through the micro crack, the subharmonics and higher harmonics will appear owing to the asymmetric stiffness interface of the micro crack. In this experiment, assuming the domain frequency shifting is result from the “CAN” effect, the largest subharmonic should appear at 80 mm-height, where nonlinear effect is strongest (β and γ are largest). However, the experimental results do not accord with this case. Thus, considering the 100 mm-height point is corresponded to the bottom boundary of the macro crack, where the ultrasonic waves suffer strongest absorption and scatter, and the proportion of high-frequency components decreased obviously in Fig. 15.

4.4. Wave velocity in cracked concrete

In order to verify the nonlinear parameters β and γ are more sensitive to the micro scale damage than traditional ultrasonic method, the

results of wave velocity tests are given in this section. The wave velocity at each test point of cracked specimens are shown in Fig. 16. The wave velocity remains constant for the first three detection points, and its maximum variation is only 4%. After macro crack appearing, the wave velocity drops significantly, and its variation rate is nearly 10%. The results show once again that traditional wave velocity method merely has ability to detect macro scale damage in concrete, while it is ineffective to characterize micro structure changes.

5. Discussion

The experimental results reported in this paper allow us to make a few considerations for a more accurate understanding of the damage degree along height of the cracked concrete specimens.

β (γ) vary with the detection point along the crack. To further confirm the presence of macro damage above the 100 mm-height, more analyses have been carried out with a wave velocity test. Table 5 shows the wave velocities obtained at different heights of the cracked specimens. The average wave velocities measured at 40, 60 and 80 mm-height points are larger than those at 120, 140 and 160 mm-height. Wave velocity is known to vary only slightly when micro scale defects are present in materials [44,45]. Therefore, being velocity variation large, it is clear that the crack above 100 mm-height should be essentially defined at macro scale. In summary, damage at different scales is distributed along crack height. At the height of 0–60 mm, the sources of nonlinearity are mainly from the weak joints between coarse aggregates and mortar (at micron scale) and other original defects formed in concrete manufacturing process [46]. Then more micro damages appear at 80 mm-height affected by the upper crack introduction, where the material continuity is affected. A macro scale crack is generated at the height of 100–200 mm of the concrete specimen, although partly closed.

We also analysed the relation between macro crack angle and wave velocity. It can be observed (Fig. 17) that with the increase of the crack angle, the wave velocity tends to decrease, which is consistent with existing research [47].

6. Conclusion

In this experiment, the scanning method is used to explore the regularity of the dependence of second- and third-order nonlinear parameters on the internal micro-scale damage of concrete. For this purpose, an effective testing system is established, and a total of 65 sets of nonlinear ultrasonic tests are carried out in this study.

It demonstrates that the nonlinear parameters β and γ show significant dependence on the test position, and that the β and γ obviously grow at a high rate once micro cracks appear. The dependence of β and γ on the test position reflects the sensibility of this method. Results of experiment allows us to speculate that the damage degree is not always at the micro scale for any ultrasound propagation path. Therefore, the higher harmonic ratios method is more suitable for long term health monitoring of the concrete structure, due to the fact that detection position do not need to change frequently. It also reveals that no obvious regularity is found for the macro scale crack detection with β and γ. The test results also show the value of β and γ is extendedly depend on the amplitude of excitation voltage: β and γ decrease with the increase of the excitation voltage when the excitation voltage at 500, 750 and 1000 V levels, respectively. The results of this experiment also show the regularity of the dependence of nonlinear parameters on crack orientation with respect to the ultrasound propagation direction, indicating that the crack orientation should be considered in characterizing micro damage in concrete with β and γ. The average increase of β at 80-mm height of the cracked specimen reaches 148%, and of γ reaches 247%, which indicates that γ is more sensitive to micro damage.

Further in depth research of this topic should be performed, e.g. using air-coupled receiver to avoid coupling error. Besides, a more extensive statistical analysis is needed to better support our conclusion. In any case, the sensibility of nonlinear ultrasonic technique has widely proven, and the robustness and stability will be particularity important in further research.

Acknowledgements

The research in this manuscript is funded by National Natural Science Foundation of China (Grant Nos. 51879017 & 51609027), Fund Projects of National Engineering Research Center for Inland Waterway Regulation Development (Grant No. SLK2017B05), Chongqing Research Program of Basic Research and Frontier Technology (Grant No. cstc2017jcyjBX0066), and Chongqing Innovative Research Program for Graduates. (Grant No. CYB17127). The tests are supported by the Key Laboratory of Water Conservancy and Water Transportation of the Ministry of Education, Chongqing Jiaotong University. We appreciate any institutions and individuals that have provided support for this paper.

References

[1] Ł. Skarżyński, J. Tejchman, Experimental investigations of fracture process in concrete by means of X-ray micro-computed tomography, Strain 52 (2016) 26–45.
[2] D. Fukuda, Y. Nara, Y. Kobayashi, M. Maruyama, M. Koketsu, D. Hayashi, H. Ogawa, K. Kaneko, Investigation of self-sealing in high-strength and ultra-low-permeability concrete in water using micro-focus X-ray CT, Cem. Concr. Res. 42 (2012) 1494–1500.
[3] M.B. Leite, P.J.M. Monteiro, Microstructural analysis of recycled concrete using X-ray microtomography, Cem. Concr. Res. 81 (2016) 38–48.
[4] F. Schubert, Numerical time-domain modeling of linear and nonlinear ultrasonic wave propagation using finite integration techniques–theory and applications, Ultrasonics 42 (2004) 221–229.
[5] P. Antonaci, C.L.E. Bruno, A.S. Gliozzi, M. Scalerandi, Monitoring evolution of compressive damage in concrete with linear and nonlinear ultrasonic methods, Cem. Concr. Res. 40 (2010) 1106–1113.
[6] G.P.M. Fierro, D. Calla, D. Ginzburg, F. Ciampa, M. Meo, Nonlinear ultrasonic stimulated thermography for damage assessment in isotropic fatigued structures, J. Sound Vib. 404 (2017) 102–115.
[7] K.H. Matlack, J.Y. Kim, L.J. Jacobs, J. Qu, Review of second harmonic generation measurement techniques for material state determination in metals, J. Nondestr. Eval. 34 (2015) 273.
[8] T. Suzuki, A. Hikata, C. Elbaum, An harmonicity due to glide motion of dislocations, J. Appl. Phys. 35 (1964) 2761–2766.
[9] A. Hikata, B.B. Chick, C. Elbaum, Dislocation contribution to the second harmonic generation of ultrasonic waves, J. Appl. Phys. 36 (1965) 229–236.
[10] A.K. Singh, B.Y. Chen, V.B.C. Tan, T.E. Tay, H.P. Lee, Finite element modeling of nonlinear acoustics/ultrasonics for the detection of closed delaminations in composites, Ultrasonics 74 (2016) 89–98.
[11] H. Sohn, H.J. Lim, M.P. Desimio, K. Brown, M. Derriso, Nonlinear ultrasonic wave modulation for online fatigue crack detection, J. Sound Vib. 333 (2014) 1473–1484.
[12] G. Kim, J.Y. Kim, K.E. Kurtis, L.J. Jacobs, Y.L. Pape, M. Guimaraes, Quantitative evaluation of carbonation in concrete using nonlinear ultrasound, Mater. Struct. 49 (2016) 399–409.
[13] S.B. Gebrekidan, T. Kang, H.J. Kim, S.J. Song, Nonlinear ultrasonic characterization of early degradation of fatigued Al6061-T6 with harmonic generation technique, Ultrasonics 85 (2017) 23–30.
[14] G. Kim, J.Y. Kim, K.E. Kurtis, L.J. Jacobs, Drying shrinkage in concrete assessed by nonlinear ultrasound, Cem. Concr. Res. 92 (2017) 16–20.
[15] J.H. Cantrell, Ultrasonic harmonic generation from fatigue-induced dislocation substructures in planar slip metals and assessment of remaining fatigue life, J. Appl. Phys. 106 (2009) 093516–93521.
[16] T.M. Apple, J.H. Cantrell, C.M. Amaro, C.R. Mayer, W.T. Yost, S.R. Agnew, J.M. Howe, Acoustic harmonic generation from fatigue-generated dislocation substructures in copper single crystals, Phil. Mag. 93 (2013) 2802–2825.
[17] I. Solodov, N. Krohn, G. Busse, Nonlinear ultrasound: a novel approach to flaw detection and imaging, Nondestruct. Testing Mater. Struct. 6 (2011) 585–591.
[18] L.A. Ostrovsky, S.N. Gurbatov, J.N. Didenkulov, Nonlinear acoustics in Nizhni Novgorod (A review), Acoust. Phys. 51 (2005) 114–127.
[19] D. Broda, W.J. Staszewski, A. Martowicz, T. Uhl, V.V. Silberschmidt, Modelling of nonlinear crack–wave interactions for damage detection based on ultrasound—a review, J. Sound Vib. 333 (2014) 1097–1118.
[20] Y. Zhao, Y. Qiu, L.J. Jacobs, J. Qu, A micromechanics model for the acoustic nonlinearity parameter in solids with distributed microcracks, AIP Conf. Proc. 1706 (2016) 060001.
[21] T. Nam, T. Lee, C. Kim, K.Y. Jhang, N. Kim, Harmonic generation of an obliquely incident ultrasonic wave in solid–solid contact interfaces, Ultrasonics 52 (2012) 778–783.

[22] J.M.C. Ongpeng, W.C. Oreta, Effect of load pattern in the generation of higher harmonic amplitude in concrete using nonlinear ultrasonic test, J. Adv. Concr. Technol. 14 (2016) 205–214.
[23] P. Antonaci, C.L.E. Bruno, P.G. Bocca, M. Scalerandi, A.S. Gliozzi, Nonlinear ultrasonic evaluation of load effects on discontinuities in concrete, Cem. Concr. Res. 40 (2010) 340–346.
[24] J.M.C. Ongpeng, A.W.C. Oreta, S. Hirose, Investigation on the sensitivity of ultrasonic test applied to reinforced concrete beams using neural network, Appl. Sci. 8 (2018) 405.
[25] S. Hirose, J.D. Achenbach, Higher harmonics in the far field due to dynamic crack-face contacting, J. Acoust. Soc. Am. 93 (2016) 142–147.
[26] M.A. Breazeale, J. Philip, Determination of third-order elastic constants from ultrasonic harmonic generation measurement, Phys. Acoust. 17 (1984) 1–60.
[27] Z. Nie, K. Wang, M. Zhao, Application of wavelet and EEMD joint denoising in nonlinear ultrasonic testing of concrete, Adv. Mater. Sci. Eng. 2018 (2018) 1–11.
[28] JGJ 55-2011, Specification for Mix Proportion Design of Ordinary Concrete, China Architecture and Building Press, 2011.
[29] J. Chen, C.L. Yang, Q.Q. Guo, Evaluation of surface cracks of bending concrete using a fully non-contact air-coupled nonlinear ultrasonic technique, Mater. Struct. 51 (2018) 104.
[30] S. Biwa, S. Nakajima, N. Ohno, On the acoustic nonlinearity of solid-solid contact with pressure-dependent interface stiffness, J. Appl. Mech. 71 (2004) 508–515.
[31] Y. Ishii, S. Biwa, Acoustic harmonic generation in a multilayered structure with nonlinear interfaces, Am. Inst. Phys. 1474 (2012) 223–226.
[32] A.A. Shah, Y. Ribakov, Non-linear ultrasonic evaluation of damaged concrete based on higher order harmonic generation, Mater. Des. 30 (2009) 4095–4102.
[33] C. Woodward, K.R. White, D.V. Jauregui, J. Stauffer, Nonlinear ultrasonic evaluation of concrete microcracking, AIP Conf. Proc. 700 (2004) 1022–1026.
[34] Y. Yang, C.T. Ng, A. Kotousov, Influence of crack opening and incident wave angle on second harmonic generation of Lamb waves, Smart Mater. Struct. 27 (2018).
[35] I. Navarrete, M. Lopez, Estimating the segregation of concrete based on mixture design and vibratory energy, Constr. Build. Mater. 122 (2016) 384–390.
[36] K. Ahmad, I.J. Smalley, Observation of particle segregation in vibrated granular systems, Powder Technol. 8 (1973) 69–75.
[37] D.K. Panesar, B. Shindman, The effect of segregation on transport and durability properties of self consolidating concrete, Cem. Concr. Res. 42 (2012) 252–264.
[38] B. Yang, S. Wei, K.Y. Shi, Modelling of multi-stage nonlinear interaction of micro-crack and ultrasonic based on equivalent elastic modulus, Acta Physica Sinica 66 (2017) 134301.
[39] P. Daponte, F. Maceri, R.S. Olivito, Ultrasonic signal-processing techniques for the measurement of damage growth in structural materials, IEEE Trans. Instrum. Meas. 44 (1995) 1003–1008.
[40] P.A. Gaydecki, F.M. Burdekin, W. Damaj, D.G. John, The propagation and attenuation of medium-frequency ultrasonic waves in concrete: a signal analytical approach, Meas. Sci. Technol. 3 (1992) 126–134.
[41] S.F. Selleck, E.N. Landis, M. Peterson, S.P. Shah, J.D. Achenbach, Ultrasonic investigation of concrete with distributed damage, ACI Mater. J. 3 (1992) 126–134.
[42] I.Y. Solodov, N. Krohn, G. Busse, CAN: an example of nonclassical acoustic nonlinearity in solids, Ultrasonics 40 (2002) 621–625.
[43] D. Ginzburg, F. Ciampa, G. Scarselli, M. Meo, SHM of single lap adhesive joints using subharmonic frequencies, Smart Mater. Struct. 26 (2017).
[44] H.J. Yim, J.H. Kim, S.J. Park, H.G. Kwak, Characterization of thermally damaged concrete using a nonlinear ultrasonic method, Cem. Concr. Res. 42 (2012) 1438–1446.
[45] A.A. Shah, Y. Ribakov, C.H. Zhang, Efficiency and sensitivity of linear and nonlinear ultrasonics to identifying micro and macro-scale defects in concrete, Mater. Des. 50 (2013) 905–916.
[46] K.L. Scrivener, A.K. Crumbie, P. Laugesen, The interfacial transition zone (ITZ) between cement paste and aggregate in concrete, Interf. Sci. 12 (2004) 411–421.
[47] J.J.S. de Figueiredo, J. Schleicher, R.R. Stewart, N. Dyaur, Estimating fracture orientation from elastic-wave propagation: an ultrasonic experimental approach, J. Geophys. Res. 117 (2012) B08304.